European Conference on Computational Fluid Dynamics
ECCOMAS CFD 2006
P. Wesseling, E. Oñate, J. Périaux (Eds)

NUMERICAL INVESTIGATION OF THE AERODYNAMIC NOISE FROM A FORWARD-FACING STEP

Young J. Moon*, Young Min Bae†, and Mun Hwan Cho†

*†Korea University,
Department of Mechanical Engineering,
1 Anam-dong, Sungbuk-ku, Seoul, 136-701, Korea
e-mail: *yjmoon@korea.ac.kr, †oioooo@korea.ac.kr, †nijih@korea.ac.kr
Web page: http:\\cfd.korea.ac.kr

Key words: Large Eddy Simulation, Linearized Perturbed Compressible Equations (LPCE), Filtered Proper Orthogonal Decomposition, Noise Source Identification

Abstract. *In the present study, aerodynamic noise from a forward-facing step is numerically investigated for Reynolds number based on the step height, Re_h=8,000 and flow Mach number, M=0.03. A three-dimensional flow over the forward-facing step is calculated by the incompressible large eddy simulation (LES), while its acoustic field is solved by the linearized compressible perturbed equations (LPCE). The space-time characteristics of the surface pressure over the step and the flow strucuture low-dimensionalized by a filtered proper orthogonal decomposition (POD) method indicate two different noise generation mechanisms at St=0.1 & 0.4~0.8. The low frequency noise is generated by a flapping motion of the shear layer. The high frequency noise is, however, generated by the breaking-off of the shear layer, due to the Kelvin-Helmholtz instability. A dominant noise source for the forward-facing step with an extended span will be expected to be around the step-corner (step front-face and leading-edge over the step) rather than near the shear layer reattachment point because the spanwise coherence length for the shear layer flapping mode is much longer than that for the shear layer breaking-off mode.*

1 INTRODUCTION

A forward-facing step which can easily be found in most of the aerodynamic vehicles or structures plays an important role in noise generation. A backward-facing step has extensively been studied at least for the flow field but the forward-facing step problem is relatively new in the study of flow[1-6] and acoustics. Recently, an experimental study[7] was conducted to find the noise source by examining the correlations between flow and acoustics. The investigation is still on-going and no decisive conclusions have been made yet.

In the present study, aerodynamic noise from a forward-facing step is numerically investigated for Reynolds number based on the step height, Re_h=8,000 and flow Mach number, M=0.03. A three-dimensional flow over the forward-facing step is solved by the incompressible large eddy simulation (LES), in which the spectral characteristics of the leading-edge separation bubble over the step need to be resolved to properly represent the noise sources.

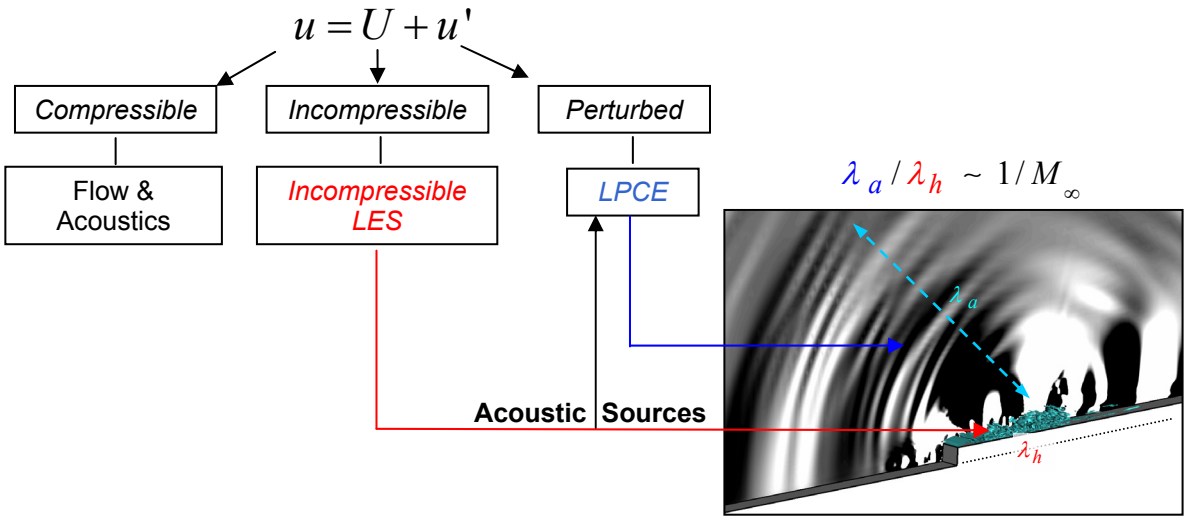

Figure 1: Computational methodology for prediction of turbulent flow noise at low Mach numbers

The acoustic field is then calculated by the linearized perturbed compressible equations (LPCE)[8], with the acoustic source and hydrodynamic flow variables computed from the incompressible large eddy simulation. A 2D LPCE calculation is conducted at zero spanwise wave-number (k_z=0), with an assumption of statistical homogeneity in the spanwise direction. The 2D acoustic computation is valid because the monitoring position for the acoustics at r=40h is not in the far-field.

Finally, the space-time characteristics of the surface pressure over the step and the filtered proper orthogonal decomposition (POD) method[9] are used to identify the noise sources and also to explain the sound generation mechanisms. The filtered-POD is useful to low-dimensionalize the flow structure by temporal and spatial filterings at a selected freuency bandwidth with a limited number of POD modes. In order to select the frequency of interest, space-time characteristics of the wall pressure over the step are examined.

2 COMPUTATIONAL METHODOLOGY

In the present study, a three-dimensional flow field is computed by the incompressible large eddy simulation (LES), while its two-dimensional acoustic field is predicted by the linearized perturbed compressible equations (LPCE) at zero spanwise wavenumber, k_z=0, with acoustic source, *DP/Dt* acquired from the incompressible LES solutions. The computational methodology is schematically represented by Fig. 1.

A. Incompressible LES/LPCE Hybrid Method

An aerodynamic noise prediction method for long-span bodies starts with computing a low Mach number turbulent flow field by incompressible LES. This is based on a hydrodynamic/

acoustic splitting method, in which the total flow variables are decomposed into the incompressible and perturbed compressible variables as,

$$\begin{aligned}\rho(\vec{x},t) &= \rho_0 + \rho'(\vec{x},t)\\ \vec{u}(\vec{x},t) &= \vec{U}(\vec{x},t) + \vec{u}'(\vec{x},t)\\ p(\vec{x},t) &= P(\vec{x},t) + p'(\vec{x},t)\end{aligned} \quad . \tag{1}$$

The incompressible variables represent hydrodynamic turbulent flow field, while acoustic fluctuations and other compressibility effects are resolved by perturbed quantities denoted by $(')$.

The incompressible LES equations are the filtered incompressible Navier-Stokes equations written as

$$\frac{\partial \tilde{U}_j}{\partial x_j} = 0 \tag{2}$$

$$\rho_0 \frac{\partial \tilde{U}_i}{\partial t} + \rho_0 \frac{\partial}{\partial x_j}(\tilde{U}_i \tilde{U}_j) = -\frac{\partial \tilde{P}}{\partial x_i} + \mu_0 \frac{\partial}{\partial x_j}\left(\frac{\partial \tilde{U}_i}{\partial x_j} + \frac{\partial \tilde{U}_j}{\partial x_i}\right) - \rho_0 \frac{\partial}{\partial x_j} M_{ij}, \tag{3}$$

where the resolved quantities are denoted by $(\tilde{\ })$ and the unknown sub-grid tensor M_{ij} is modeled as

$$M_{ij} = \widetilde{U_i U_j} - \tilde{U}_i \tilde{U}_j = -(C_s \Delta)^2 \left|\tilde{S}\right| \tilde{S}_{ij} \,. \tag{4}$$

Here, Δ is the mean radius of a grid cell (computed as the cubic root of its volume). For solving the filtered incompressible Navier-Stokes equations, an iterative fractional-step method is used. The governing equations are spatially discretized with a sixth-order compact scheme[10] to avoid excessive numerical dissipations and dispersions errors and integrated in time by a four-stage Runge-Kutta method. The 10th-order spatial filtering of Gaitonde et al.[11] is also applied to enhance the numerical stability with high frequency cutoff.

To calculate the acoustics, the perturbed compressible equations (PCE)[12,13] are derived by subtracting the incompressible Navier-Stokes equations from the compressible ones. The PCE, however, yields errors excited by the perturbed vorticity ($\vec{\omega}' = \nabla \times \vec{u}'$), if $\vec{\omega}'$ is not properly resolved with the acoustic grid. This error is even more pronounced, as Reynolds number increases. Thereby, the linearized perturbed compressible equations (LPCE) are proposed by present authors. In LPCE, evolution of perturbed vorticity is pre-suppressed in the formulation, deliberating the fact that the perturbed vorticity has little effect on the noise generation at low Mach numbers. A set of LPCE can be written in a vector form as,

$$\frac{\partial \rho'}{\partial t} + (\vec{U} \cdot \nabla)\rho' + \rho_0 (\nabla \cdot \vec{u}') = 0 \tag{5}$$

$$\frac{\partial \vec{u}'}{\partial t} + \nabla(\vec{u}' \cdot \vec{U}) + \frac{1}{\rho_0}\nabla p' = 0 \tag{6}$$

$$\frac{\partial p'}{\partial t} + (\vec{U} \cdot \nabla) p' + \gamma P(\nabla \cdot \vec{u}') + (\vec{u}' \cdot \nabla) P = -\frac{DP}{Dt}. \tag{7}$$

The LPCE is linearized to a base incompressible flow field and its formulation is much simpler than the original PCE. Because a curl of the linearized perturbed momentum equations, Eq. (6) yields

$$\frac{\partial \vec{\omega}'}{\partial t} = 0, \tag{8}$$

LPCE consequently prevents any further changes (generation, convection, and decaying) of perturbed vorticity in time. It also provides a physical base for using large grid spacing near the wall because they are in an invisicd form. Details on derivation of LPCE and characteristics of the perturbed vorticity can be found in reference[8]. The LPCE has been validated for a laminar tone from a circular cylinder at Re_D=150 and M=0.1 and also the vortex sound problems at high Reynolds numbers – quadruple sound of Kirchhoff vortex and temporal mixing layer noise[8].

The left hand side of LPCE represents effects of acoustic wave propagation and refraction in an unsteady, inhomogeneous flow, while the right hand side only contains the acoustic source term. The sources are projected from the hydrodynamic flow solution, using a bi-linear shape function. It is interesting to note that for low Mach number flows, the total change of the hydrodynamic pressure, *DP/Dt* is considered as the only explicit noise source term.

2.2 Filtered proper orthogonal decomposition

The proper orthogonal decomposition (POD) method can be applied to extract principle components of the complex field mathematically. The complex turbulent flow field can also be analyzed by the POD method. In POD, an arbitrary field in time and space, $u(\vec{x},t)$ is decomposed into eigen-modes(n), i.e. time coefficient $a_n(t)$ and spatial eigen-function $\psi_n(\vec{x})$

$$u(\vec{x},t) = \sum_{n=1}^{\infty} a_n(t)\psi_n(\vec{x}). \tag{9}$$

The spatial eigen-function, $\psi_n(\vec{x})$ represents the n-th dominant modal shape and its time variations are represented by $a_n(t)$. Equation (9) can be transformed into an eigen-value problem of auto-correlation matrix

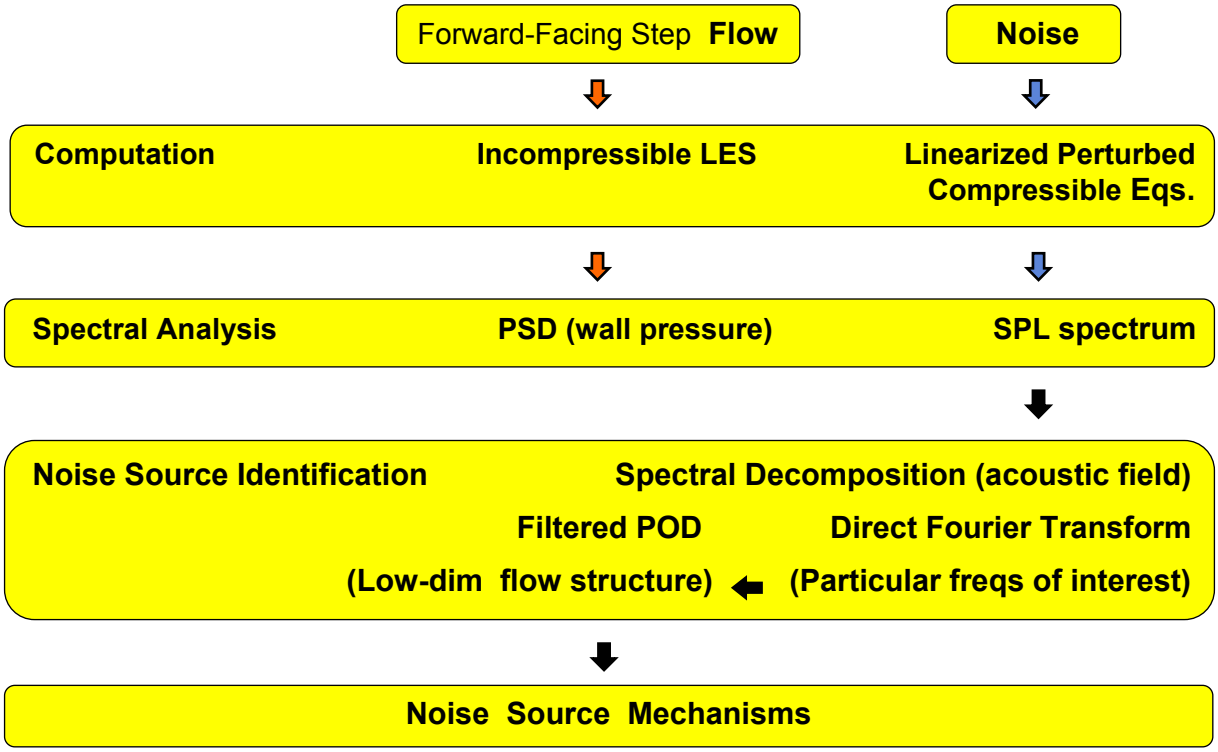

Figure 2: Noise source identification method

$$\int < u(\vec{x}) \cdot u^*(\vec{x'}) > \psi_n(\vec{x'}) d\vec{x'} = \lambda_n \psi_n(\vec{x'}), \tag{10}$$

where $< >$ denotes a time-average and λ_n is the n-th eigen-value. In a discretized two-dimensional domain (N×M), Eq. (10) can be rewritten as,

$$[< u(i:j) \cdot u(i':j') > \omega(i':j')][\psi_n(i':j')] = \lambda_n [\psi_n(i:j)], \tag{11}$$

where i=1…N, j=1…M, i'=1…N, j'=1…M, and $\omega(i':j')$ is the optimal weighting for an integration over the domain. The size of auto-correlation matrix is (N×M)×(N×M) and ψ_n is the vector with length of (N×M). From Eq. (11), the spatial eigen-function $\psi_n(\vec{x})$ can be obtained. The time coefficients are then calculated by

$$a_n(t) = u(\vec{x}, t) \cdot \psi_n(\vec{x}). \tag{12}$$

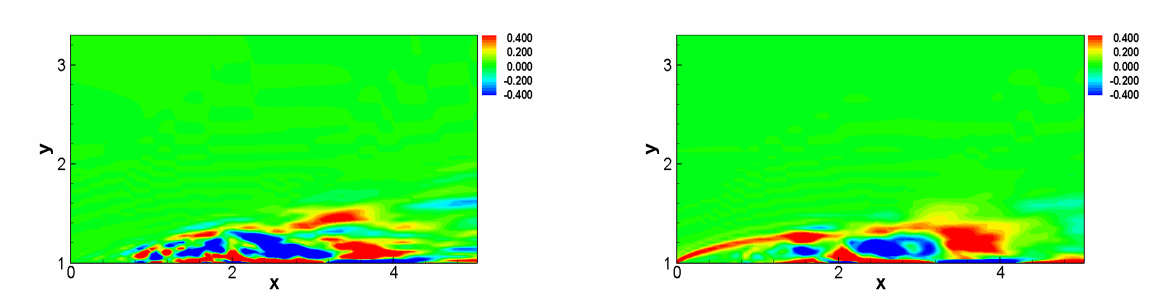

a) b)

Figure 3: Comparison of spectrally decomposed vorticity field (spanwise-averaged) at *St*=0.1; a) direct Fourier transform, b) filtered POD (w/ 20 eignemodes)

The $\psi_n(\vec{x})$ and $a_n(t)$ have to satisfy

$$\int \psi_m(\vec{x}) \cdot \psi_l(\vec{x}) d\vec{x} = \delta_{ml}, \tag{13}$$

and

$$\int a_m(t) \cdot a_l(t) dt = \lambda_l \delta_{ml}. \tag{14}$$

To extract the filtered structure at a certain frequency, the frequency coefficients are obtained by the Fourier-transform of the time coefficient

$$\hat{a}_n(\omega) = \int a_n(t) \exp(-i\omega t) dt. \tag{15}$$

The field in frequency domain is then given by reconstruction of each eigen-mode as

$$\hat{u}(\vec{x}, \omega) = \sum_{n=1}^{\infty} \hat{a}_n(\omega) \psi_n(\vec{x}). \tag{16}$$

In the present study, a limited number of modes n=1~20 are used for spatial simplification. Finally, the filtered structure in frequency range $\omega_a \leq \omega \leq \omega_b$ of our interests is calculated via an inverse-Fourier transform

$$\tilde{u}(\vec{x}, t)_{ab} = \int_{\omega_b}^{\omega_a} \hat{u}(\vec{x}, \omega) \exp(i\omega t) d\omega. \tag{17}$$

Figure 3 compares two spectrally filtered vorticity fields near the reattachment point of the shear layer: one with the direct Fourier transform and the other with the filtered-POD. The latter clearly represents much identifiable, low-dimensionalized flow structures, compared to the former.

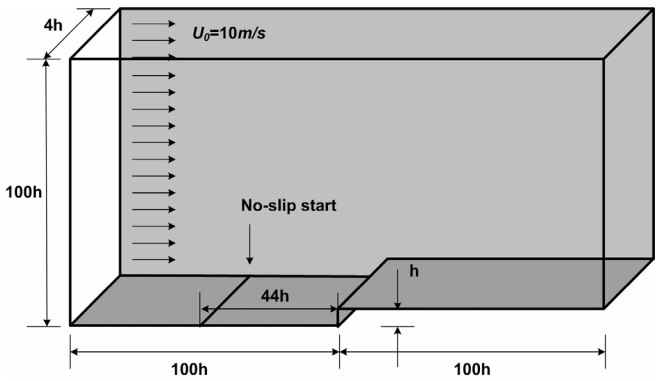

Figure 4: Numerical set-up for the forward facing step

3 RESULTS AND DISCUSSION

3.1 Flow and acoustics

The flow and acoustics over the forward-facing step are computed for Reynolds number based on a step height (h=0.012m), Re_h=8000 and free stream Mach number, M_a=0.03 (U_o=10m/s). As depicted in Fig. 4, the hydrodynamic computational domain for incompressible LES is extended from -100h to 100h in the streamwise direction, from 0 to 100h in the normal direction, and 4h in the spanwise direction. A no-slip boundary condition is applied at x=-44h, where a laminar boundary layer starts to develop and a flow periodicity is assumed at the spanwise boundaries. The non-uniform cartesian grids consist of 3.8 million grid points with minimum normal grid spacing, 0.002h. The computational domain is decomposed into 62 blocks for parallel computation with 31×41×51 points in x-, y-, and z-directions for each block.

A laminar boundary layer separates before the step and at the step corner. The shear layer emanated from the corner-edge becomes unstable at this Reynolds number and immediately

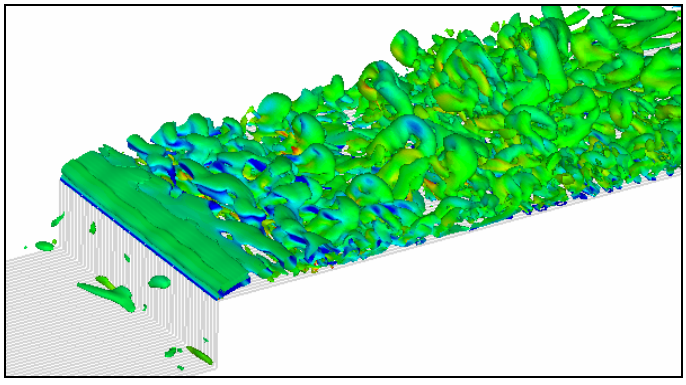

Figure 5: Instantaneous eddy structures over the step (Q=0.5)

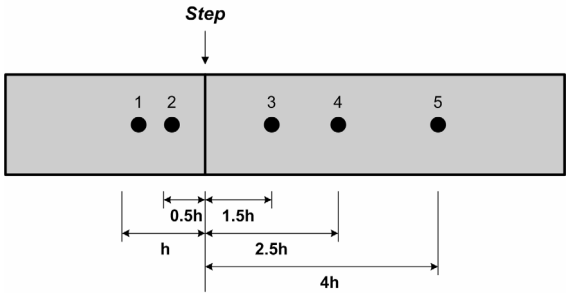

Figure 6: Monitoring points for the wall pressure fluctuations

transits to turbulences. The iso-surfaces of Q in Fig. 5 clearly show the highly three-dimensional instantaneous eddy structures over the step. By Kelvin-Helmholtz instability, the shear layer at the leading-edge is breaking off into smaller eddies, convecting downstream with a speed of $0.67U_o$ (see Fig. 11(a)). After the reattachment point, developments of hair-pin vortices in the boundary layer are clearly discernable and flow is expected to become a turbulent boundary layer (TBL). It is also interesting to notice the 'spanwise' instability of the shear layer, which will be more discussed later, in connection with the low frequency noise.

The wall pressure fluctuations are monitored at various positions: pos. 1 and 2 are under and 3, 4, and 5 are over the step (see Fig. 6), and Fig. 7 shows the wall pressure fluctuation spectra at the corresponding monitoring positions. One clear distinction is that the wall pressure spectra at pos. 1 and 2 show a peak at St=0.1, while at pos. 3, 4, and 5 (near the reattachment point), the spectrum becomes much broadended, e.g. plateu up to St=0.5 and

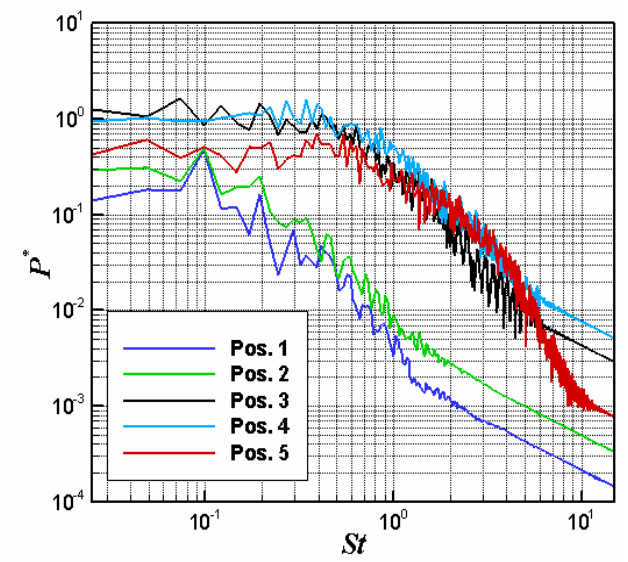

Figure 7: Wall pressure spectra at monitoring positions

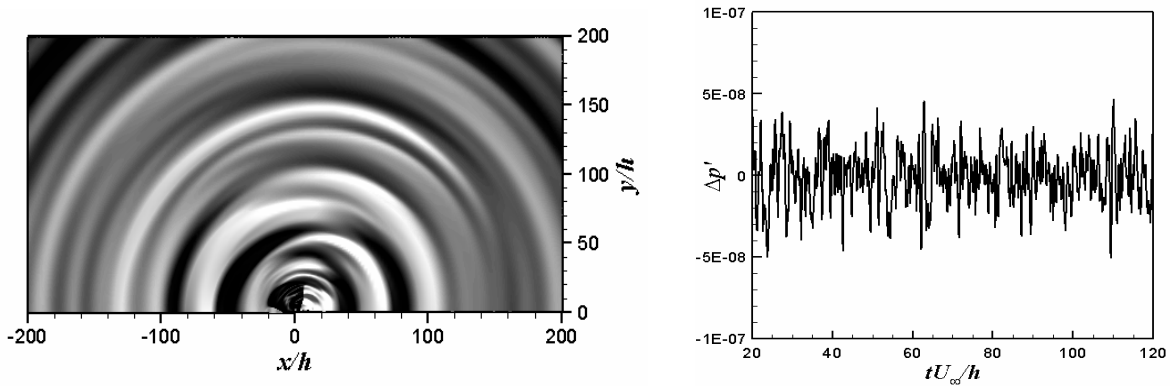

Figure 8: Instantaneous pressure fluctuation field over the step and time variation of $\Delta p'$ at r=40h vertically sway from the step edge

gradually decaying at higher frequencies (present calculation has a time resolution only up to St=5). Also, the overall spectrum level at pos. 3, 4, and 5 is significantly lifted. One may expect that the wall pressure fluctuations near the reattachment point are the noise sources but it is difficult to pin-point the sources.

Now, a two-dimensional acoustic calculation is conducted by LPCE with the spanwise-averaged hydrodynamic flow variables and acoustic source term, DP/Dt at the zero spanwise wave-number, k_z=0. This is based on an assumption of statistical homogeneity in the spanwise direction. The acoustic grid consists of 541×181 points distributed in the domain of 400h×200h with minimal normal grid spacing at the wall ten times larger than that of the hydrodynamic grid. The methodology described above is computationally efficient for low Mach number aeroacoustics.

Figure 8 shows an instantaneous pressure fluctuation field ($\Delta p' = p - \overline{p}$) over the forward facing step and its time variation at r=40h vertically away from the step edge. As shown in the wall pressure spectra (see Fig. 7), sound waves are generated by sources with a wide range of scales. Figure 9 shows a directivity of $\Delta p'_{rms}$ at the same radial position, indicating a

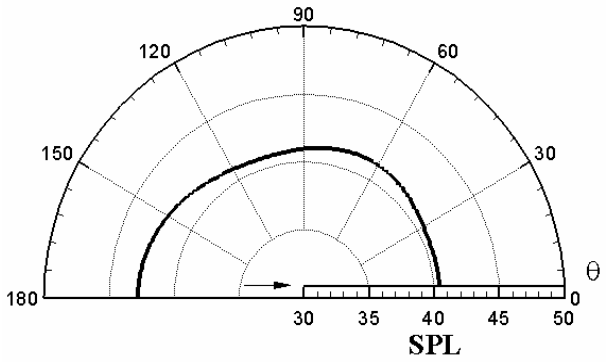

Figure 9: Directivity pattern of $\Delta p'_{rms}$ at r=40h with a center at (0,h)

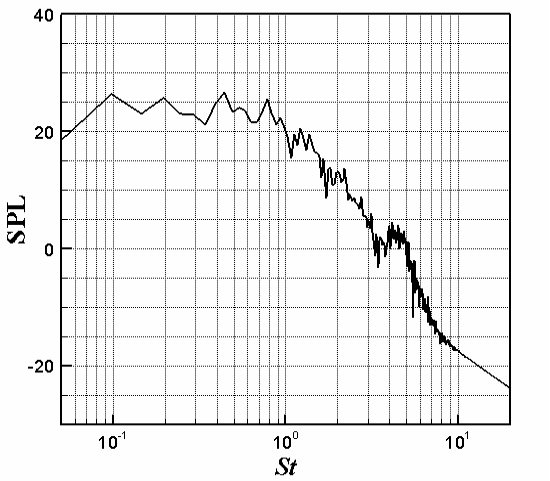

Figure 10: Sound pressure level spectrum at r=40h vertically away from the step edge

somewhat pronounced effect at $120^{o} < \theta < 180^{o}$. Also, the computed SPL spectrum is presented in Fig. 10. The spectrum is quite broadband and similar to the wall pressure spectra near the reattachment of the shear layer over the step. So, our conjecture on the noise source was correct, i.e. near the leading-edge separation bubble. On the other hand, its noise generation mechanism is yet to be identified, especially the effects associated with the step-edge.

3.2 Noise source identification

The SPL spectrum shown in Fig. 10 indicates major sound sources in the frequency range from St=0.1 to 0.8, i.e. a plateu region. In order to identify the sources, space-time characteristics

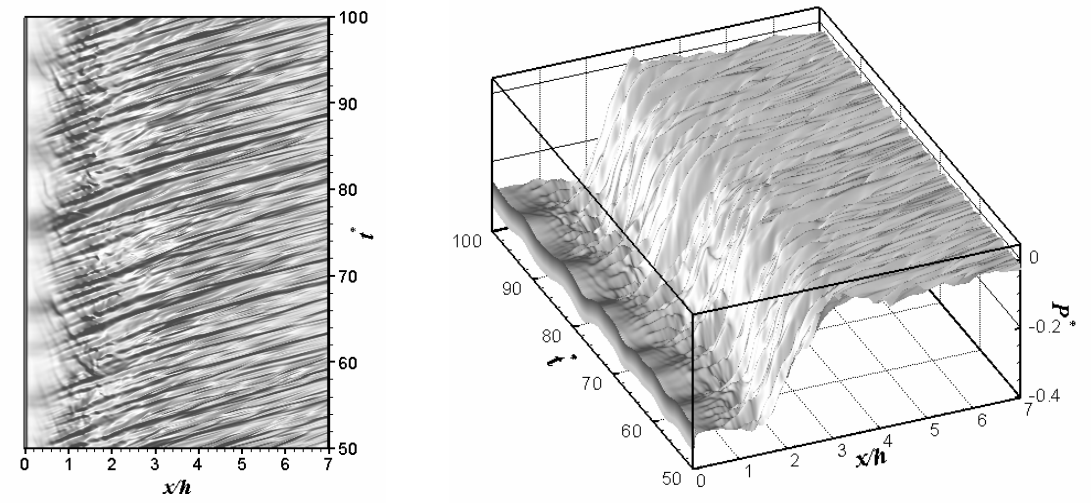

Figure 11: Space-time characteristics of the wall pressure fluctuations

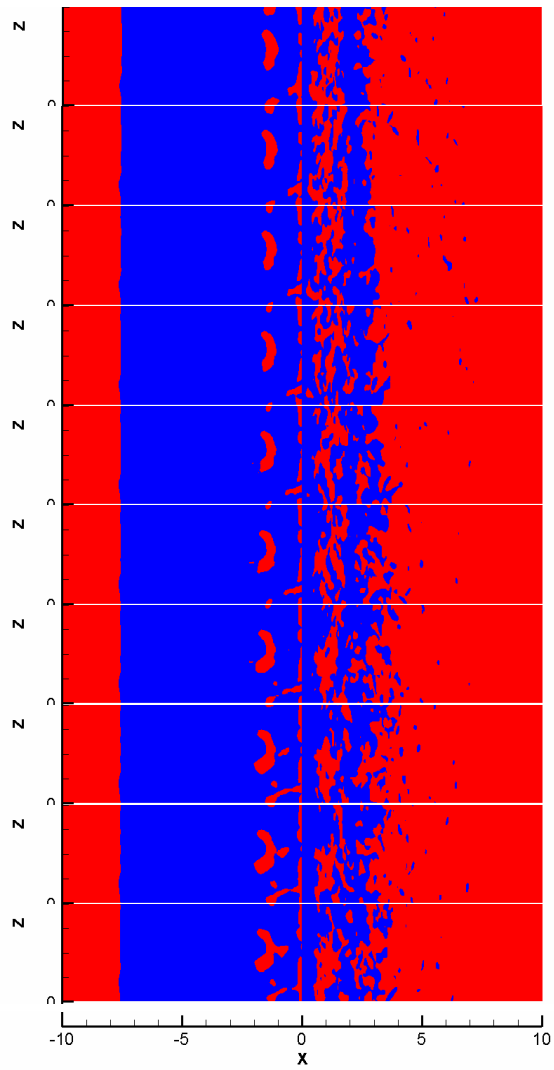

Figure 12: Wall-shear stress contours: 10 frames over a time period corresponding to St=0.1 (blue: negative, red: positive, the step-edge starts at x=0, x & z are normalized by h)

of the wall pressure fluctuations over the step are plotted in the streamwise direction (see Fig. 11). One can notice that the shear layer is breaking-off into various smaller-scale eddies at x=h but two time-scales at St=0.4-0.5 and St=0.8-0.9 are more clearly identifiable. They also convect downstream with a speed of approximately $0.67U_o$ but the eddy structure at St=0.4-0.5 is most coherent among various eddy-scales. This frequency coincides with the most unstable mode[14] in the shear layer instability, i.e. at $\omega\delta/c$=0.42 (or St=0.5). Here, ω is the angular frequency, δ is the shear layer thickness, and c is the convection velocity.

Also, one can notice a distinct pattern of pressure fluctuations at St=0.1 between the leading-edge of the step and x/h=1. These low frequency fluctuations are better visualized in a

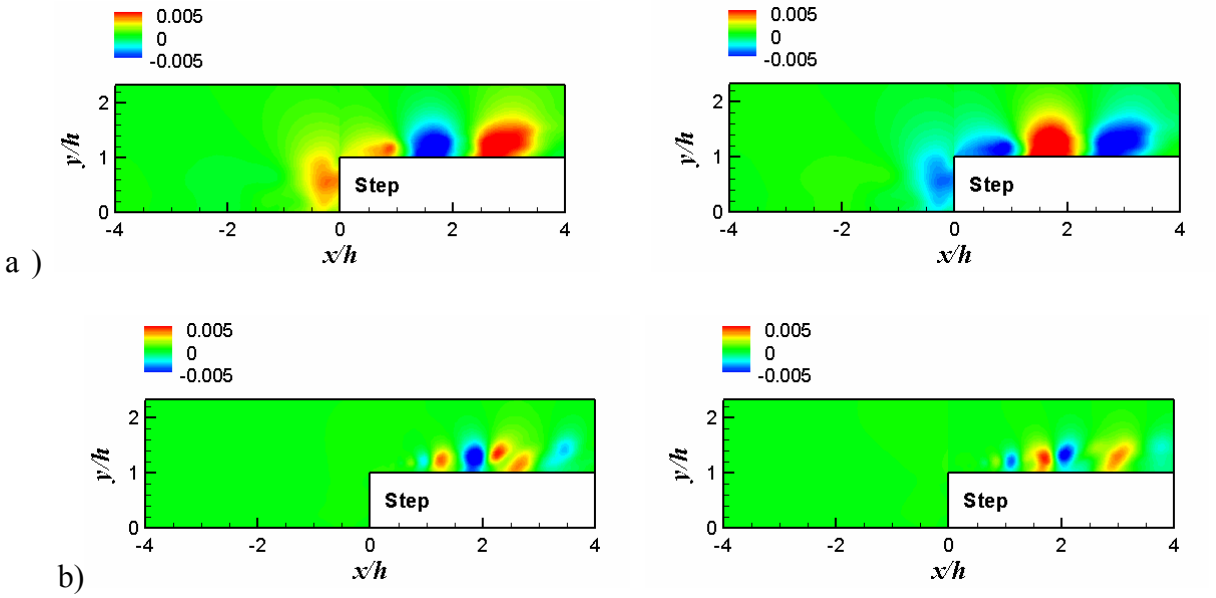

Figure 13: Instantaneous hydrodynamic pressure fluctuation filtered at two frequencies by POD with a limited number of eigen-modes: a) St=0.1, b) St=0.45

perspective view of the *x-t* plot (right). These low frequency fluctuations seem related to the flapping motion[1-6] of the shear layer. The flapping motion of the shear layer at low frequency (e.g. *St*=0.06-0.08) has been reported in various studies of the leading-edge separation bubble. Figure 12 shows ten frames of wall-shear stress contours in a time period corresponding to *St*=0.1 (the step-edge starts from x/h=0). One can clearly see the enlargement/contraction of the separation bubble at this frequency.

Now, a filtered-POD analysis is conducted on the pressure fluctuation field over the step in an *x-y* plane. Figure 13 shows the instantaneous pressure fluctuation fields filtered at two frequencies, *St*=0.1 and 0.45, reconstructed by an inverse Fourier transform with a limited number of eigenmodes (20 eigenmodes). Figure 13(a) presents two low-dimensionalized, instantaneous pressure fluctuation fields, separated by a time period corresponding to *St*=0.1. It is clearly shown that pressure fluctuations at *St*=0.1 occur not only over the step edge ($0<x/h<1$) but also over the step front-face and they are in the same phase. The pressure fluctuations at *x/h*=1.75 and 3 (opposite phase) result from a periodic streamwise movement of the vortex core of the shear layer roll-up, i.e. flapping motion of the shear layer. This shear layer flapping is a large-scale motion, compared to the shear layer breaking-off (local occurrence). When the shear layer is elongated or contracted over the step, the vortex strength in the re-circulating zone in front of the step periodically changes and thereby the induced-pressure field must fluctuate. Meanwhile, Fig. 13(b) shows the filtered pressure fluctuation fields at *St*=0.45, which are representing the shear layer breaking-off near the reattachment point. Figures 13(a) & (b) support well the wall pressure spectra presented in Fig. 7, where pos. 1 & 2 show a dominant peak only at *St*=0.1, while pos. 3, 4, & 5 indicate a broadband profile from *St*=0.1 to 0.5.

4 CONCLUSIONS

In the present study, the aerodynamic noise from a forward-facing step is numerically investigated for Reynolds number based on the step height, Re_h=8,000 and flow Mach number, M=0.03. From the computed results, it can be concluded that

- the space-time characteristics of the surface pressure over the step and the low-dimensionalized flow strucutures by filtered proper orthogonal decomposition (POD) method indicate two different noise generation mechanisms at St=0.1 & 0.4~0.8,
- the low frequency noise is generated by a flapping motion of the shear layer, while the high frequency noise is generated by the breaking-off of the shear layer, due to the Kelvin-Helmholtz instability,
- the actual noise of forward-facing step from an extended span will be generated more dominantly from the region around the step-corner (i.e. step front-face and leading-edge over the step) rather than from a region close to the shear layer reattachment point, because the spanwise coherence length for the flapping motion of the shear layer at St=0.1 is much longer than that for the shear layer breaking-off at St=0.45.

REFERENCES

[1] M. Kiya and K. Sasaki, "Freestream turbulence effects on a separation bubble," *Journal of Wind Engineering and Industrial Aerodynamics*, Vol. 14, 375-386 (1983).

[2] M. Kiya and K. Sasaki, "Structure of a turbulent separation bubble," *Journal of Fluid Mechanics*, Vol. 137, 83-113 (1983).

[3] M. Kiya and K. Sasaki, "Structure of large-scale vortices and unsteady reverse flow in the reattaching zone of a turbulent separation bubble," *Journal of Fluid Mechanics*, Vol. 154, 463-491 (1985).

[4] R. Hillier and N.J. Cherry, "The effect of stream turbulence on separation bubbles," *Journal of Wind Engineering and Industrial Aerodynamics*, Vol. 8, 49-58 (1981).

[5] Y. Nakamura and S. Ozono, "The effects of turbulence on a separated and reattaching flow," *Journal of Fluid Mechanics*, Vol. 178, 477-490 (1987).

[6] A. Suksangpanomrung, N. Djilali, and P. Moinat, "Large-eddy simulation of separated flow over a bluff rectangular plate," *International Journal of Heat and Fluid Flow*, Vol. 21, 655-663 (2000).

[7] S. Becker, M. Escobar, C. Hahn, I. Ali, M. Kaltenbacher, B. Basel, and M. Grunewald, "Experimental and Numerical Investigation of the Flow Induced Noise from a Forward Facing Step," *AIAA-Paper* 2005-3006 (2005).

[8] J.H. Seo and Y.J. Moon, "The Linearized Perturbed Compressible Equations for Low Mach Number Aeroacoustic," *Journal of Computational Physics* (accepted) (2006).

[9] S.A.L. Glegg and W.J. Davenport, "Proper Orthogonal decomposition of Turbulent Flows for Aeroacoustic and Hydrodynamic application," *Journal of Sound and Vibration*, Vol. 239, No. 4, 767-784 (2001).

[10] S.K. Lele, "Compact Finite Difference Schemes with Spectral-Like Resolution," *Journal*

of Computational Physics, Vol. 103, 16-42 (1992).
[11] D. Gaitonde, J.S. Shang, and J.L. Young, "Practical Aspects of High-Order Accurate Finite-Volume Schemes for Electrmagnetics," *AIAA-Paper*, 97-0363 (1997).
[12] J. H. Seo and Y.J. Moon, "The Perturbed Compressible Equations for Aeroacoustic Noise Prediction at Low Mach Numbers," *AIAA Journal*, Vol. 43, No. 8, 1716-1724 (2005).
[13] Y.J. Moon and J.H. Seo, "A Splitting Method for Aeroacoustic Noise Prediction of Low Mach Number Viscous Flows," *International Journal of Aeroacoustics*, Vol. 4, No. 1, 1-16 (2005).
[14] W.K. Blake, *Mechanics of Flow-Induced Sound and Vibration, Vol. 1, General concepts and elementary sources*, Academic Press (1986).